Superconductivity in the Li-B-C system at 100 GPa

Feng Zheng,[1] Yang Sun,[1,2,3,*] Renhai Wang,[4] Yimei Fang,[1] Feng Zhang,[2,5] Shunqing Wu,[1,†] Cai-Zhuang Wang,[2,5] Vladimir Antropov,[2,5] and Kai-Ming Ho[2]

[1]*Department of Physics, OSED, Key Laboratory of Low Dimensional Condensed Matter Physics (Department of Education of Fujian Province), Jiujiang Research Institute, Xiamen University, Xiamen 361005, China*

[2]*Department of Physics, Iowa State University, Ames, Iowa 50011, USA*

[3]*Department of Applied Physics and Applied Mathematics, Columbia University, New York, New York, 10027, USA*

[4]*School of Physics and Optoelectronic Engineering, Guangdong University of Technology, Guangzhou 510006, China*

[5]*Ames Laboratory, U.S. Department of Energy, Ames, Iowa 50011, USA*

(Received 30 July 2022; accepted 3 January 2023; published 17 January 2023)

Layer Li-B-C compounds have been shown to have feasible superconductivity. Using the adaptive genetic algorithm, we predict the structures of the Li-B-C system at 100 GPa. We identify several low-enthalpy metallic phases with stoichiometries of LiB_2C, LiB_3C, Li_2BC_2, $Li_3B_2C_3$, Li_3BC, and Li_5BC. Using a fast screening method of electron-phonon interaction, we find that LiB_3C is a promising candidate for superconductivity. The consecutive calculations using the full Brillouin zone confirm the existence of the strong electron-phonon coupling (EPC) in this system. The anharmonic B-C phonon modes near the zone center provide the major contribution to the EPC. The EPC constant is 1.40, and the estimated critical temperature is 22 K. In this paper, we indicate that superconductivity can also happen without a layered structural motif in the Li-B-C system. We also demonstrate an effective strategy for crystal structure prediction of superconducting materials.

DOI: 10.1103/PhysRevB.107.014508

I. INTRODUCTION

Exploring high-temperature superconductors is an important research goal in physics, chemistry, and materials science. Inspired by the discovery of a superconducting transition ~ 40 K in the rather simple MgB_2 compound [1–3], extensive research has been conducted on its related materials [4–9] (graphitelike layered materials intercalated with alkali or alkali-earth) to obtain possible superconductors. Among them, graphitelike layered Li-B-C compounds have been the subject of sustained interest because these structures with light elements may have strong covalent bonding and significant phonon frequencies, with underlying high-T_c (conventional) superconductivity [10,11]. LiBC with $P6_3/mmc$ symmetry [12,13] has a similar crystal structure to MgB_2. However, unlike MgB_2, LiBC exhibits an insulating nature [13]. According to Bardeen-Cooper-Schrieffer (BCS) theory [14], metallicity is an important requirement for a conventional superconductor. Therefore, to achieve superconductivity in LiBC, Rosner *et al.* [15] suggested metalizing LiBC by introducing vacancies at Li sites. Based on density functional theory (DFT) calculations, they found that $Li_{0.5}BC$ becomes superconducting at ~ 100 K. However, no experimental efforts have reported superconductivity of the Li-deficient LiBC compounds >2 K [16–19]. Further research shows that the absence of superconductivity of Li_xBC can be attributed to structural instability in the B-C layer at low Li deficiency, which leads to a dramatic change in electronic structure [20]. Considering that hole doping by introducing Li vacancies will cause structural instability in Li_xBC, Gao *et al.* [5] designed a freestanding LiB_2C_2 trilayer. Due to no vacancies involved in trilayer LiB_2C_2, the structural distortion in the B-C layer may be prevented. First-principles calculations predict that this trilayer LiB_2C_2 is a superconductor with $T_c \sim 92$ K. Furthermore, partially replacing carbons with borons in LiBC-type compounds was also proposed, such as $LiB_{1.1}C_{0.9}$ [21], $Li_3B_4C_2$ [22], Li_2B_3C [22], and $Li_4B_5C_3$ [7], which have all been predicted to be superconductors. More recently, Quan *et al.* [23] reported superconductivity in the honeycomb structure $Li_{2x}BC_3$ at $x = 0.5$ by theoretical calculations. The calculated superconducting critical temperature T_c is comparable with that in MgB_2. These results show that the design of stoichiometric constituents of graphitelike layered Li-B-C compounds provides a feasible route to induce superconductivity.

So far, most attention has been focused on elucidating the nature of superconductivity of Li-B-C compounds with a graphitelike layered structure. A natural question remains whether there is any other Li-B-C structure that can lead to superconductivity. To answer this question, a comprehensive investigation of the crystal structures and superconductivity of the Li-B-C system should be carried out. These studies can help establish correlations of structural stability and superconducting properties with different structural motifs in the Li-B-C system, which in turn can be used to guide other researchers to reveal more promising superconductors. On the other hand, it has been shown that high pressure offers another effective strategy for identifying structural motifs for

*yangsun@iastate.edu
†wsq@xmu.edu.cn

superconductivity [24–27] because high-pressure conditions can enhance the interatomic interaction, tune electronic properties, and metalize materials. Furthermore, the application of pressure also can access unusual chemistry and stable structures that cannot be realized under ambient conditions [28], which may raise the possibility of finding superconducting materials. Therefore, in this paper, we investigate the structural and superconducting properties of the Li-B-C system at 100 GPa with crystal structure predictions. We employ a recently developed frozen-phonon method of electron-phonon coupling (EPC) calculations [29] to fast-screen possible Li-B-C superconductors.

II. COMPUTATIONAL METHODS

The crystal structures of B-C, Li-C, and Li-B-C at 100 GPa were determined by using the adaptive genetic algorithm (AGA) method [30], which combines fast structure exploration by auxiliary classical potentials and accurate *ab initio* calculations adaptively and iteratively. In the genetic algorithm (GA) loop, the initial atomic positions of the Li, B, and C atoms were randomly generated without any assumption on the Bravais lattice type, symmetry, atom basis, or unit cell dimensions. The total structure pool in our GA search was set to 128. The structure search with auxiliary interatomic potentials was performed in 400 consecutive GA generations. Then the 16 lowest-enthalpy structures at the end of each GA search were selected for single-point DFT calculations according to the AGA procedure [30], whose energies, force, and stress are used to adjust the interatomic potential parameters for the next iteration of GA search. A total of 40 adaptive iterations were performed to obtain the final structures.

Here, the embedded-atom method (EAM) [31] was used as a classical auxiliary potential. In EAM, the total energy of an N-atom system was evaluated by

$$E_{\text{total}} = \frac{1}{2}\sum_{i,j(i\neq j)}^{N}\phi(r_{ij}) + \sum_{i}F_i(n_i), \tag{1}$$

where $\phi(r_{ij})$ denotes the pair repulsion between atoms i and j with a distance of r_{ij}, and $F_i(n_i)$ is the embedded term with electron density term $n_i = \sum_{j\neq i}\rho_j(r_{ij})$ at the site occupied by atom i. The potential fitting is performed by the force-matching method with a stochastic simulated annealing algorithm as implemented in the POTFIT code [32,33].

First-principles calculations were performed by using the projector augmented-wave [34] representations with DFT as implemented in the Vienna *Ab initio* Simulation Package [35,36]. The exchange and correlation energy was treated within the spin-polarized generalized gradient approximation and parameterized by the Perdew-Burke-Ernzerhof (PBE) formula [37]. Wave functions were expanded in plane waves up to a kinetic energy cutoff of 520 eV. Brillouin zone integrations were approximated using special k-point sampling of the Monkhorst-Pack scheme [38] with a k-point mesh resolution of $2\pi \times 0.03\,\text{Å}^{-1}$. Lattice vectors and atomic coordinates were fully relaxed until the force on each atom was $< 0.01\,\text{eV Å}^{-1}$. The fast screening of EPC constant λ_Γ at the Brillouin zone center was carried out based on the frozen-phonon method [29]. The zone-center phonon was computed by the PHONOPY software [39,40], with a finer $k-$point sampling grid of $2\pi \times 0.02\,\text{Å}^{-1}$ spacing and a criterion of self-consistent calculation 10^{-8} eV.

The full Brillouin zone EPC calculations were performed with the QUANTUM ESPRESSO code [41,42] based on density-functional perturbation theory (DFPT) [43]. The ultrasoft pseudopotentials from the PSLibrary1.0.0 (high accuracy) [44] for the PBE functional were used, with $2s^1$, $2s^2\,2p^1$, and $2s^2\,2p^2$ as valence electrons of Li, B, and C, respectively. The kinetic energy cutoffs were 75 Ry for wave functions and 576 Ry for potentials. The charge densities were determined on a k mesh of $24 \times 24 \times 24$. The dynamical matrices were calculated on a q mesh of $6 \times 6 \times 6$. The convergence threshold for self-consistency was 1×10^{-12} Ry.

The calculations of superconducting T_c are based on the Eliashberg spectral equation $\alpha^2F(\omega)$ [45,46] defined commonly now as

$$\alpha^2F(\omega) = \frac{1}{2\pi N(E_f)}\sum_{q\upsilon}\frac{\gamma_{q\upsilon}}{\hbar\omega_{q\upsilon}}\delta(\omega-\omega_{q,\upsilon}), \tag{2}$$

where $N(E_f)$ is the density of states (DOS) at the Fermi level, $\omega_{q\upsilon}$ denotes the phonon frequency of the mode υ with wave vector $\mathbf{q}$, and $\gamma_{q\upsilon}$ is the phonon linewidth defined as

$$\gamma_{q\upsilon} = \frac{2\pi\omega_{q\upsilon}}{\Omega_{\text{BZ}}}\sum_{ij}\int d^3k\left|g^{ij}_{k,q\upsilon}\right|^2\delta(\epsilon_{q,i}-E_f)\delta(\epsilon_{k+q,j}-E_f), \tag{3}$$

where $\epsilon_{q,i}$ and $\epsilon_{k+q,j}$ are eigenvalues of Kohn-Sham orbitals at given bands and vectors, $\mathbf{q}$ and $\mathbf{k}$ are wave vectors, and i and j denote indices of energy bands. Here, $g^{ij}_{k,q\upsilon}$ is the EPC matrix element, which describes the probability amplitude for the scattering of an electron with a transfer of crystal momentum $\mathbf{q}$, determined by

$$g^{ij}_{k,q\upsilon} = \left(\frac{\hbar}{2M\omega_{q\upsilon}}\right)^{1/2}\left\langle\Psi_{i,k}\left|\frac{dV_{\text{SCF}}}{d\hat{\mu}_{q\upsilon}}\hat{e}_{q\upsilon}\right|\Psi_{i,k+q}\right\rangle, \tag{4}$$

where M is the atomic mass, $\hat{e}_{q\upsilon}$ is the phonon eigenvector, $dV_{\text{SCF}}/d\hat{\mu}_{q\upsilon}$ measures the change of self-consistent potential induced by atomic displacement, and $\Psi_{i,k}$ and $\Psi_{i,k+q}$ are Kohn-Sham orbitals. The EPC constant λ can be determined through summation over the first Brillouin zone or integration of the spectral function in frequency space:

$$\lambda = \sum_{q\upsilon}\lambda_{q\upsilon} = 2\int\frac{\alpha^2(\omega)}{\omega}d\omega, \tag{5}$$

where the EPC constant $\lambda_{q\upsilon}$ for mode υ at wave vector $\mathbf{q}$ using Eq. (5) can be written as

$$\lambda_{q\upsilon} = \frac{\gamma_{q\upsilon}}{\pi\hbar N(E_f)\omega^2_{q\upsilon}}. \tag{6}$$

The superconducting T_c is determined with the analytical McMillan equation modified by the Allen-Dynes formula [47,48]:

$$T_c = \frac{\omega_{\log}}{1.2}\exp\left[\frac{-1.04(1+\lambda)}{\lambda(1-0.62\mu^*)-\mu^*}\right], \tag{7}$$

where μ^* is the effective screened Coulomb repulsion constant whose values are generally between 0.1 and 0.15 [49,50],

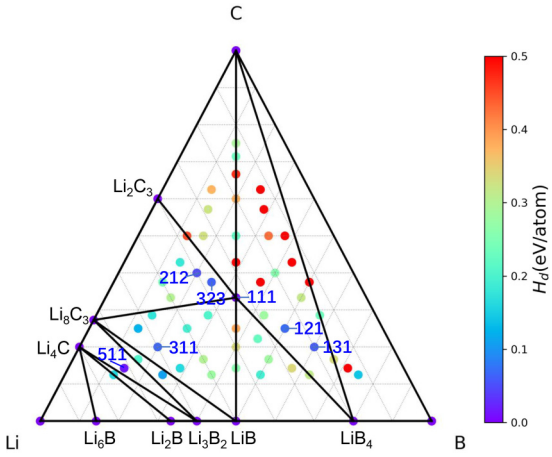

FIG. 1. The convex hull of the Li-B-C system at 100 GPa.

and $\omega_{\log}$ is the logarithmic average frequency:

$$\omega_{\log} = \exp\left[\frac{2}{\lambda}\int \frac{d\omega}{\omega}\alpha^2 F(\omega)\ln\omega\right]. \quad (8)$$

III. RESULTS AND DISCUSSION

A. AGA search of Li-B-C ternary phases at 100 GPa

Before we discuss ternary compounds in the Li-B-C system, the structural stability of elements and binary phases should first be clarified. At 100 GPa, calculations show that the ground-state phases of elemental Li, B, and C adopt *Pbca* [51,52], *Cmca* ($\alpha-$Ga structure) [53], and $Fd\bar{3}m$ (diamond) [54] symmetries, respectively. For the Li-B binary phase, because previous crystal structure searches [55,56] have already covered the pressure used in this paper, we did not perform additional structure searches of Li-B compounds. We recalculated the enthalpies of these crystal structures. Our results show that five compounds with Li_6B ($R\bar{3}$), Li_2B (*Cmcm*), Li_3B_2 ($R\bar{3}m$), LiB ($Fd\bar{3}m$), and LiB_4 ($I4/mmm$) are stable at 100 GPa. For the B-C compounds, Jay *et al.* [57] investigated from ambient pressure to 80 GPa. We performed the AGA search at 100 GPa and found no B-C binary compound was stable at 100 GPa, like the high-pressure results of Jay *et al.* [57]. For the Li-C system, our AGA searches indicate that Li_4C ($P2_1/c$), Li_8C_3 ($R\bar{3}m$), and Li_2C_3 (*Cmcm*) compounds are the ground-state phases at 100 GPa. More details of AGA searches in B-C and Li-C systems can be found in the Supplemental Material [58]. The stable crystal structures of these elements and binary phases are shown in Fig. S3 in the Supplemental Material [58], and their structural parameters are listed in Supplemental Material Table S1 [58].

In Fig. 1, we present ternary compounds of Li-B-C at 100 GPa from the AGA searches. For simplicity, all chemical formulae are expressed as Li : B : C reduced ratios. For example, 111 represents the compound with LiBC. During the structural search, we select a range of different stoichiometries (i.e., 111, 112, 121, 211, 113, 122, 131, 212, 221, 311, 114, 123, 132, 141, 213, 231, 312, 321, 411, 115, 124, 133, 142, 151, 214, 223, 232, 241, 313, 322, 331, 412, 421, 511, 116, 125, 134, 143, 152, 161, 215, 233, 251, 314, 323, 332, 341, 413, 431, 512, 521, and 611) with 2 or 4 formula units to perform the AGA search. The relative stability of these predicted Li-B-C compounds was investigated under the corresponding pressure, depending on the calculated formation enthalpies:

$$H_f = \frac{H(\mathrm{Li}_x\mathrm{B}_y\mathrm{C}_z) - xH(\mathrm{Li}) - yH(\mathrm{B}) - zH(\mathrm{C})}{x+y+z}, \quad (9)$$

where H ($\mathrm{Li}_x\mathrm{B}_y\mathrm{C}_z$) is the total enthalpy of the $\mathrm{Li}_x\mathrm{B}_y\mathrm{C}_z$ compound. Here, H (Li), H (B), and H (C) are the enthalpies of the ground states of Li, B, and C at 100 GPa. Also, H_d is introduced as the enthalpy above the convex hull to represent the relative stability on the phase diagram. Ground-state phases have $H_\mathrm{d} = 0$.

As shown in Fig. 1, LiBC is the only ternary ground-state compound at 100 GPa. The crystal structure is the same as the experimental structure of LiBC ($P6_3/mmc$ symmetry) determined by Wörle *et al.* [12] at ambient pressure. This indicates that the ambient-pressure LiBC phase is stable up to 100 GPa, which agrees with previous studies [59]. Figure 2(a) shows the atomic structure of hexagonal LiBC at 100 GPa. This structure is the same as MgB_2 with alternating graphenelike B-C and Li layers. The detailed structural parameters are listed in Supplemental Material Table S2 [58]. The calculated phonon spectrum confirms that this phase is dynamically stable at 100 GPa (Supplemental Material, Fig. S4(a) [58]). The electronic DOS in Fig. S4(b) in the Supplemental Material [58] shows that LiBC is in an insulating phase at 100 GPa.

In addition to the ternary ground-state LiBC structure, we also identify a few low-enthalpy metastable structures with enthalpy very close to the convex hull ($H_\mathrm{d} < 100$ meV/atom), namely, LiB_2C, LiB_3C, Li_2BC_2, $Li_3B_2C_3$, Li_3BC, and Li_5BC. The H_d are so small that these compounds may be realized in experiments. We compute the Gibbs free energy of formation for one of the structures (LiB_3C) to examine the effect of temperature on structural stability with the quasiharmonic approximation. The results suggest that the temperature may improve the stability of LiB_3C (see Supplemental Material Note 2 [58]). The crystal structures of these Li-B-C compounds are shown in Figs. 2(b)–2(g). The LiB_2C in Fig. 2(b) adopts the orthorhombic structure with *Cmcm* symmetry. This structure is a three-dimensional framework with PbO-type [60] layers of B_2 and C chains separated by Li atoms, which is like *Cmcm* $CeNiSi_2$. The *Cm* LiB_3C also has a PbO-type layered motif of B_3C, and Li atoms locate between two PbO-type layers, as shown in Fig. 2(c). This structure is like the $BaFe_2As_2$ phase [61]. The Li_2BC_2 (*Pbam*) and $Li_3B_2C_3$ (*Pm*) in Figs. 2(d)–2(e) both have B-C layered structures with 5- and 8-membered rings and 5-, 6- and 8-membered rings, respectively. The *Cm* Li_3BC [Fig. 2(f)] is found to form B-C nanoribbons structure, while for $P-1$ Li_5BC [Fig. 2(g)], B and C atoms connect to form chains. The structural parameters of these phases are listed in Supplemental Material Table S2 [58]. Figures S5–S10 in the Supplemental Material [58] show the phonon dispersions and DOS for these metastable Li-B-C phases. The results show that, unlike insulating LiBC, these low-enthalpy Li-B-C compounds are metallic. Furthermore, phonon calculations confirm that these Li-B-C compounds are dynamic stability at 100 GPa. It should be noted that the LiB_3C structure has minor imaginary frequencies near the Γ point (Supplemental Material, Fig. S6(a) [58]). However, it

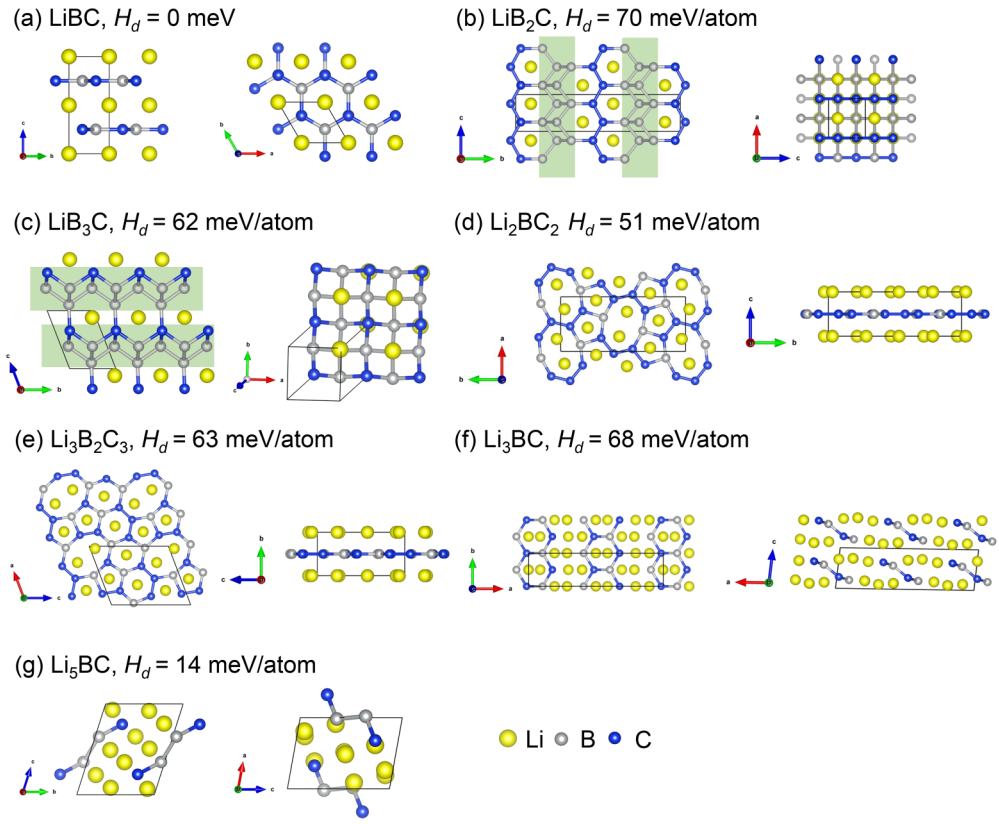

FIG. 2. Atomic structures of (a) $P6_3/mmc$ LiBC, (b) $Cmcm$ LiB_2C, (c) Cm LiB_3C, (d) $Pbam$ Li_2BC_2, (e) Pm $Li_3B_2C_3$, (f) Cm Li_3BC, and (g) $P-1$ Li_5BC at 100 GPa. The light green rectangle denotes PbO-type motifs.

does not mean the dynamical instability of this material. Since the phonon calculations are based on the harmonic approximation, the presence of imaginary phonon frequencies may also be associated with a strongly anharmonic effect, which will be discussed later.

B. Fast screening of superconductivity of Li-B-C compounds

Motivated by the metallic properties of these metastable Li-B-C compounds, we further investigated their superconductivity. To determine the phonon-mediated superconductivity, it is usually based on the calculations of EPC in the

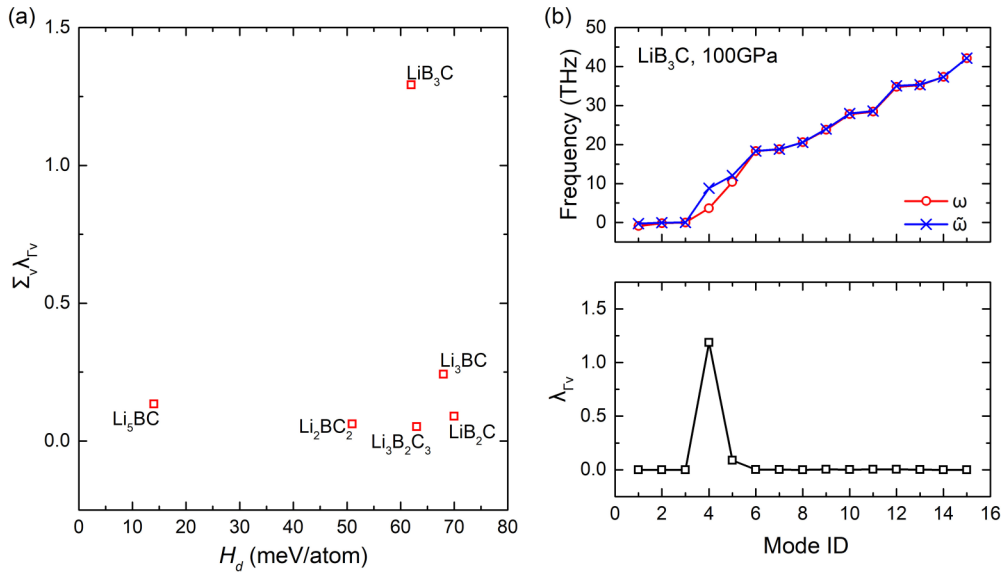

FIG. 3. (a) The enthalpy above the convex hull (H_d) vs electron-phonon coupling (EPC) constant $\sum_v \lambda_{\Gamma v}$ at the Brillouin zone center. (b) The screened and unscreened phonon frequency (top panel) and zone-center EPC strength (bottom panel) in the LiB_3C phase at 100 GPa.

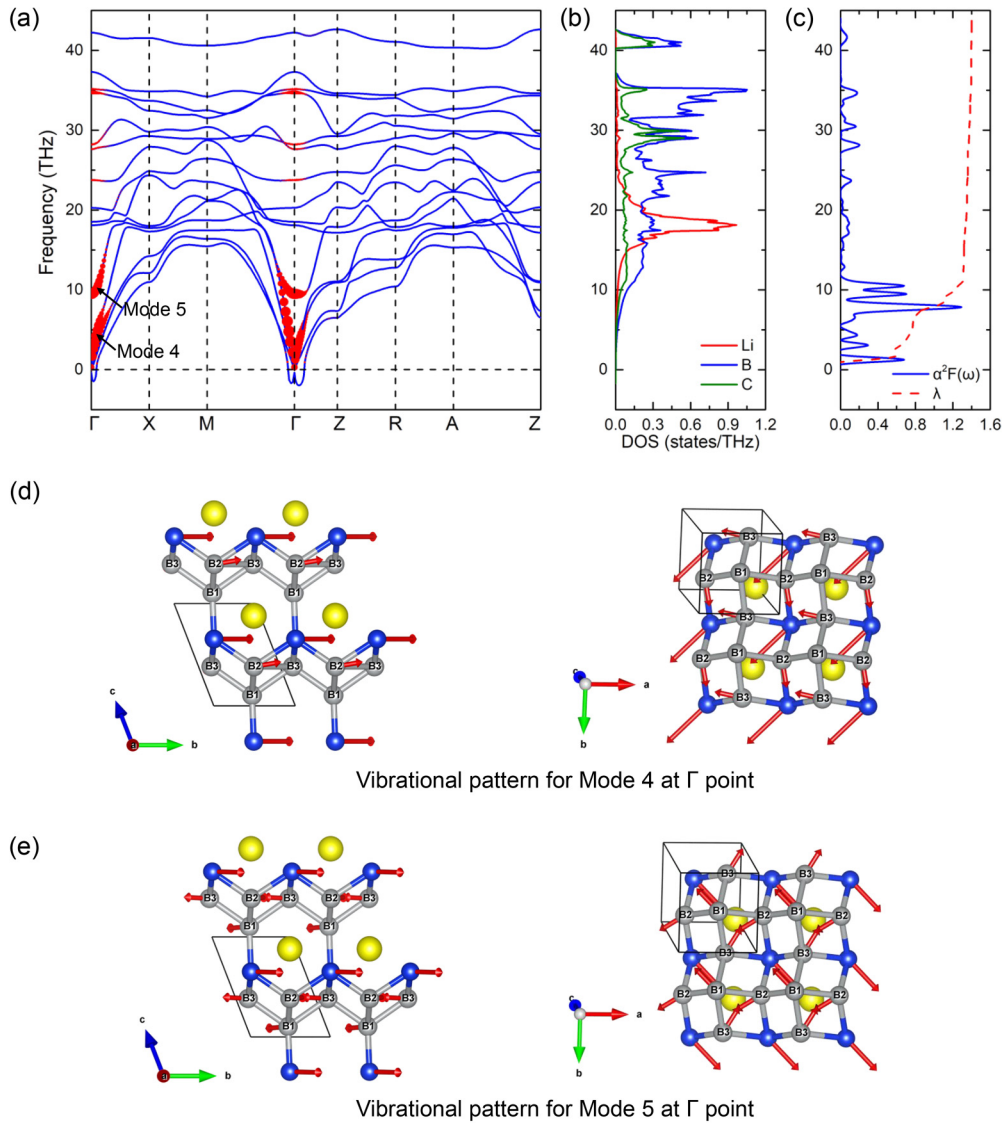

FIG. 4. (a) Phonon spectrum of LiB_3C. Red solid circles represent the phonon linewidth (γ_{qv}) with a radius proportional to the strength. (b) Projected phonon density of states (DOS). (c) Eliashberg spectral function $\alpha^2F(\omega)$ with integrated electron-phonon coupling (EPC) parameter $\lambda(\omega)$. The vibrational patterns for (d) mode 4 and (e) mode 5 at the Γ point.

full Brillouin zone. However, these calculations are time consuming, particularly in complicated systems, which impedes high-throughput superconducting materials studies. Therefore, we first employ a fast screening of these phases with the zone-center EPC strength λ_Γ based on the frozen-phonon method [29]. Here, λ_Γ can be defined by

$$\lambda_{\Gamma v} = \frac{\tilde{\omega}^2_{\Gamma v} - \omega^2_{\Gamma v}}{4\omega^2_{\Gamma v}}, \tag{10}$$

where $\omega_{\Gamma v}$ and $\tilde{\omega}_{\Gamma v}$ are screened and unscreened phonon frequencies of mode v at zone-center, respectively. Using this method, we find only LiB_3C has a high $\sum_v \lambda_{\Gamma v}$ (the summation of zone-center EPC of all modes), as shown in Fig. 3(a). The high $\sum_v \lambda_{\Gamma v}$ of LiB_3C can be attributed to the large difference between screened and unscreened phonon frequencies of modes 4 and 5, as shown in Fig. 3(b).

To further quantify the electron-phonon interaction in LiB_3C, we investigate its EPC with full Brillouin zone calculations. Figure 4(a) shows the γ_{qv}-weighted phonon spectrum with DFPT calculations. Now one can see that phonon modes 4 and 5 have a large contribution to the phonon linewidth and correspondingly to the electron-phonon interaction near the Γ point, which agrees well with the fast screening results. These two modes mainly involve vibrations of boron and carbon atoms, as shown in Fig. 4(b). Their vibrational configurations at the Γ point are shown in Figs. 4(d) and 4(e), respectively. Mode 4 corresponds to stretching vibrations of B2, B3, and C atoms in the a–b plane. For mode 5, B2-B3 atoms and B1-C atoms both show symmetric stretching vibrations in the a–b plane. The calculated Eliashberg function $\alpha^2F(\omega)$ is shown in Fig. 4(c). The integrated EPC parameter λ is 1.40. The $\omega_{\log}$ can be obtained from Eq. (8), which is 197.31 K. We predict $T_c = 22$ K ($\mu^* = 0.1$) for LiB_3C. As a comparison, we also compute the full EPC for the LiB_2C phase with *Cmcm*

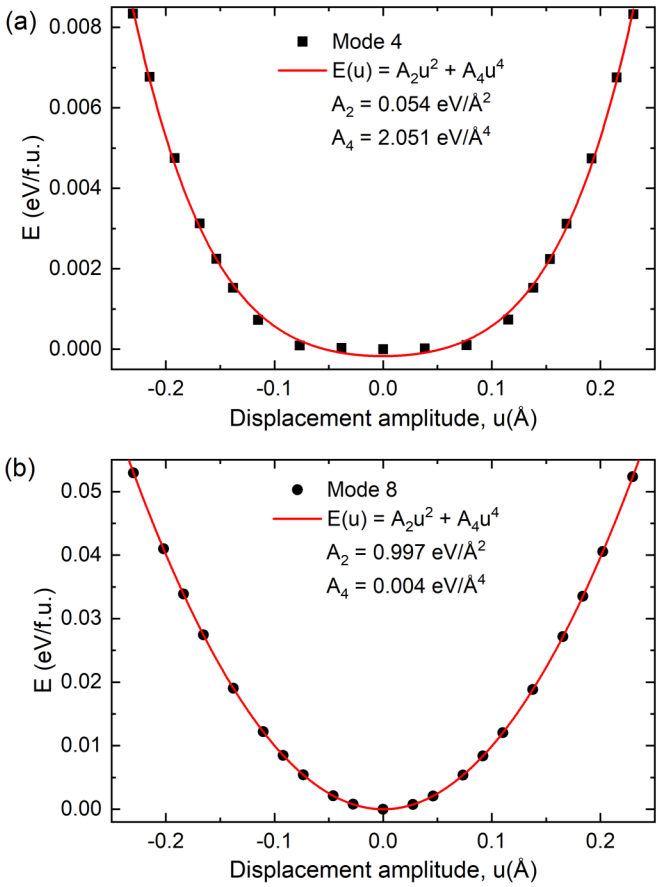

FIG. 5. Frozen-phonon calculation of the total energy change as a function of atomic displacement for two zone-center modes. (a) The anharmonic mode 4 and (b) harmonic mode 8. The red curve shows the fitting.

symmetry, which is not expected to show a strong EPC from zone-center EPC calculations. We obtain $\lambda = 0.37$ and $T_c = 3$ K ($\mu^* = 0.1$) for LiB_2C (see Fig. S12 in the Supplemental Material [58]), indicating the accuracy of the zone-center EPC screening method.

C. Anharmonic effect of LiB_3C

As mentioned above, there are small imaginary phonon frequencies contributed in LiB_3C, shown in Figs. 4(a) and S6(a) in the Supplemental Material [58]. Specifically, we find the frequency of mode 4 shows a strong dependence on the magnitude of displacement in the frozen-phonon calculations. To further investigate this behavior, we calculated the energy changes as all atoms displaced along the eigenmodes of mode 4 at the Γ point in Fig. 5. The displacement for atom i is $\mathbf{D}_i = u\frac{v_i}{\sqrt{m_i}}$, where u is the displacement amplitude, v_i is the eigenvector, and m_i is the atomic mass. To compare, we also plot mode 8, which is a harmonic mode mainly contributed by the Li vibration. Compared with the harmonic mode, the potential well of mode 4 is very flat at small displacement and increases rapidly at large displacement. It can only be fit to $E(u) = A_2u^2 + A_4u^4$ with a vanishing A_2 and a large A_4, as shown in Fig. 5(a). This indicates that mode 4 has unusually large anharmonicity, and the conventional harmonic phonon calculations are in a nonpertubative regime. Therefore, the current harmonic energy, 1.10 THz or 4.56 meV, should be much lower than the actual energy. The correct treatment of anharmonic effects on superconductivity can be complicated, but such large anharmonicity has been seen previously, and its influence on EPC and T_c has also been discussed in the literature [62,63]. The EPC constant λ can be expected to generally be somewhat smaller. However, the influence of this change on T_c is not unique due to the significant increase of $\omega_{\log}$ when the anharmonicity is included. Due to such cancellation effects, different formulas can produce the increase or decrease of T_c; however, overall, this effect seems to be small [62]. The phonon dispersions of LiB_3C are also computed at 0 and 50 GPa (see Fig. S13 in the Supplemental Material [58]). No negative frequency is found, suggesting that LiB_3C is dynamically stable at low pressures.

IV. CONCLUSIONS

In summary, we use the AGA method to study the Li-B-C system at 100 GPa. We identify several low-enthalpy metallic phases with stoichiometries of LiB_2C, LiB_3C, Li_2BC_2, $Li_3B_2C_3$, Li_3BC, and Li_5BC. By a fast evaluation of zone-center electron-phonon interactions in these metallic Li-B-C structures, we identify that LiB_3C can be a promising candidate for superconductivity. The calculations of EPC in the full Brillouin zone and analysis with the Eliashberg function $\alpha^2F(\omega)$ verify the superconductivity of LiB_3C with EPC constant $\lambda = 1.40$ and $T_c = 22$ K. The electron-phonon interactions are mainly contributed by low-frequency anharmonic phonon modes involving vibrations of boron and carbon atoms. Our results indicate rich structural motifs in the Li-B-C system at high pressure, and the superconductivity in this system can happen in the phases without layered structure. In this paper, we also demonstrate an effective strategy to combine crystal structure prediction and fast screening for conventional superconductors that can be used in many other systems.

ACKNOWLEDGMENTS

Work at Xiamen University was supported by the National Natural Science Foundation of China (Grant No. 11874307). R.W. was supported by the Guangdong Basic and Applied Basic Research Foundation (Grants No. 2021A1515110328 and No. 2022A1515012174). Y.S. and V.A. were supported by National Science Foundation Award No. DMR-2132666. C.-Z.W. and F.Z. were supported by the U.S. Department of Energy (DOE), Office of Science, Basic Energy Sciences, Materials Science and Engineering Division. Ames Laboratory is operated for the U.S. DOE by Iowa State University under Contract No. DE-AC02-07CH11358, including the grant of computer time at the National Energy Research Supercomputing Center in Berkeley.

[1] J. Nagamatsu, N. Nakagawa, T. Muranaka, Y. Zenitani, and J. Akimitsu, Nature (London) **410**, 63 (2001).

[2] Y. Kong, O. V. Dolgov, O. Jepsen, and O. K. Andersen, Phys. Rev. B **64**, 020501(R) (2001).

[3] T. Yildirim, O. Gulseren, J. W. Lynn, C. M. Brown, T. J. Udovic, Q. Huang, N. Rogado, K. A. Regan, M. A. Hayward, J. S. Slusky *et al.*, Phys. Rev. Lett. **87**, 037001 (2001).

[4] N. Emery, C. Herold, M. d'Astuto, V. Garcia, C. Bellin, J. F. Mareche, P. Lagrange, and G. Loupias, Phys. Rev. Lett. **95**, 087003 (2005).

[5] M. Gao, X.-W. Yan, Z.-Y. Lu, and T. Xiang, Phys. Rev. B **101**, 094501 (2020).

[6] E. Haque, M. A. Hossain, and C. Stampfl, Phys. Chem. Chem. Phys. **21**, 8767 (2019).

[7] T. Bazhirov, Y. Sakai, S. Saito, and M. L. Cohen, Phys. Rev. B **89**, 045136 (2014).

[8] T. E. Weller, M. Ellerby, S. S. Saxena, R. P. Smith, and N. T. Skipper, Nat. Phys. **1**, 39 (2005).

[9] W. Hayami and T. Tanaka, AIP Advances **10**, 065213 (2020).

[10] J. M. An and W. E. Pickett, Phys. Rev. Lett. **86**, 4366 (2001).

[11] S. Di Cataldo, S. Qulaghasi, G. B. Bachelet, and L. Boeri, Phys. Rev. B **105**, 064516 (2022).

[12] M. Wörle, R. Nesper, G. Mair, M. Schwarz, and H. G. Vonschnering, Z. anorg. allg. Chem. **621**, 1153 (1995).

[13] P. F. Karimov, N. A. Skorikov, E. Z. Kurmaev, L. D. Finkelstein, S. Leitch, J. MacNaughton, A. Moewes, and T. Mori, J. Phys.: Condens. Matter **16**, 5137 (2004).

[14] J. Bardeen, L. N. Cooper, and J. R. Schrieffer, Phys. Rev. **108**, 1175 (1957).

[15] H. Rosner, A. Kitaigorodsky, and W. E. Pickett, Phys. Rev. Lett. **88**, 127001 (2002).

[16] A. Bharathi, S. J. Balaselvi, M. Premila, T. N. Sairam, G. L. N. Reddy, C. S. Sundar, and Y. Hariharan, Solid State Commun. **124**, 423 (2002).

[17] D. Souptel, Z. Hossain, G. Behr, W. Loser, and C. Geibel, Solid State Commun. **125**, 17 (2003).

[18] A. M. Fogg, P. R. Chalker, J. B. Claridge, G. R. Darling, and M. J. Rosseinsky, Phys. Rev. B **67**, 245106 (2003).

[19] A. M. Fogg, J. B. Claridge, G. R. Darling, and M. J. Rosseinsky, Chem. Commun. **12**, 1348 (2003).

[20] A. M. Fogg, J. Meldrum, G. R. Darling, J. B. Claridge, and M. J. Rosseinsky, J. Am. Chem. Soc. **128**, 10043 (2006).

[21] R. Miao, J. Yang, M. Jiang, Q. Zhang, D. Cai, C. Fan, Z. Bai, C. Liu, F. Wu, and S. Ma, J. Appl. Phys. **113**, 133910 (2013).

[22] M. Gao, Z. Y. Lu, and T. Xiang, Phys. Rev. B **91**, 045132 (2015).

[23] Y. Quan and W. E. Pickett, Phys. Rev. B **102**, 144504 (2020).

[24] A. P. Drozdov, P. P. Kong, V. S. Minkov, S. P. Besedin, M. A. Kuzovnikov, S. Mozaffari, L. Balicas, F. F. Balakirev, D. E. Graf, V. B. Prakapenka *et al.*, Nature (London) **569**, 528 (2019).

[25] A. P. Drozdov, M. I. Eremets, I. A. Troyan, V. Ksenofontov, and S. I. Shylin, Nature (London) **525**, 73 (2015).

[26] M. Somayazulu, M. Ahart, A. K. Mishra, Z. M. Geballe, M. Baldini, Y. Meng, V. V. Struzhkin, and R. J. Hemley, Phys. Rev. Lett. **122**, 027001 (2019).

[27] E. Snider, N. Dasenbrock-Gammon, R. McBride, X. Wang, N. Meyers, K. V. Lawler, E. Zurek, A. Salamat, and R. P. Dias, Phys. Rev. Lett. **126**, 117003 (2021).

[28] H. K. Mao, X. J. Chen, Y. Ding, B. Li, and L. Wang, Rev. Mod. Phys. **90**, 015007 (2018).

[29] Y. Sun, F. Zhang, C.-Z. Wang, K.-M. Ho, I. I. Mazin, and V. Antropov, Phys. Rev. Mater. **6**, 074801 (2022).

[30] S. Q. Wu, M. Ji, C. Z. Wang, M. C. Nguyen, X. Zhao, K. Umemoto, R. M. Wentzcovitch, and K. M. Ho, J. Phys.: Condens. Matter **26**, 035402 (2014).

[31] S. M. Foiles, M. I. Baskes, and M. S. Daw, Phys. Rev. B **33**, 7983 (1986).

[32] P. Brommer and F. Gahler, Philos. Mag. **86**, 753 (2006).

[33] P. Brommer and F. Gahler, Modelling Simul. Mater. Sci. Eng. **15**, 295 (2007).

[34] G. Kresse and D. Joubert, Phys. Rev. B **59**, 1758 (1999).

[35] G. Kresse and J. Furthmuller, Phys. Rev. B **54**, 11169 (1996).

[36] G. Kresse and J. Furthmuller, Comp. Mater. Sci. **6**, 15 (1996).

[37] J. P. Perdew, K. Burke, and M. Ernzerhof, Phys. Rev. Lett. **77**, 3865 (1996).

[38] S. Froyen, Phys. Rev. B **39**, 3168 (1989).

[39] A. Togo, F. Oba, and I. Tanaka, Phys. Rev. B **78**, 134106 (2008).

[40] A. Togo and I. Tanaka, Scripta Mater. **108**, 1 (2015).

[41] P. Giannozzi, S. Baroni, N. Bonini, M. Calandra, R. Car, C. Cavazzoni, D. Ceresoli, G. L. Chiarotti, M. Cococcioni, I. Dabo *et al.*, J. Phys.: Condens. Matter **21**, 395502 (2009).

[42] P. Giannozzi, O. Andreussi, T. Brumme, O. Bunau, M. B. Nardelli, M. Calandra, R. Car, C. Cavazzoni, D. Ceresoli, M. Cococcioni *et al.*, J. Phys.: Condens. Matter **29**, 465901 (2017).

[43] S. Baroni, S. de Gironcoli, A. Dal Corso, and P. Giannozzi, Rev. Mod. Phys. **73**, 515 (2001).

[44] A. Dal Corso, Comp. Mater. Sci. **95**, 337 (2014).

[45] G. M. Eliashberg, Sov. Phys. JETP **11**, 696 (1960).

[46] G. M. Eliashberg, Sov. Phys. JETP **12**, 1000 (1961).

[47] P. B. Allen, Phys. Rev. B **6**, 2577 (1972).

[48] P. B. Allen and R. C. Dynes, Phys. Rev. B **12**, 905 (1975).

[49] C. F. Richardson and N. W. Ashcroft, Phys. Rev. Lett. **78**, 118 (1997).

[50] K. H. Lee, K. J. Chang, and M. L. Cohen, Phys. Rev. B **52**, 1425 (1995).

[51] J. Lv, Y. Wang, L. Zhu, and Y. Ma, Phys. Rev. Lett. **106**, 015503 (2011).

[52] C. J. Pickard and R. J. Needs, Phys. Rev. Lett. **102**, 146401 (2009).

[53] A. R. Oganov, J. H. Chen, C. Gatti, Y. Z. Ma, Y. M. Ma, C. W. Glass, Z. X. Liu, T. Yu, O. O. Kurakevych, and V. L. Solozhenko, Nature (London) **457**, 863 (2009).

[54] T. Yamanaka and S. Morimoto, Acta Cryst. B **52**, 232 (1996).

[55] F. Peng, M. Miao, H. Wang, Q. Li, and Y. Ma, J. Am. Chem. Soc. **134**, 18599 (2012).

[56] A. Hermann, A. McSorley, N. W. Ashcroft, and R. Hoffmann, J. Am. Chem. Soc. **134**, 18606 (2012).

[57] A. Jay, O. H. Duparc, J. Sjakste, and N. Vast, J. Appl. Phys. **125**, 185902 (2019).

[58] See Supplemental Material at http://link.aps.org/supplemental/10.1103/PhysRevB.107.014508 for the AGA search of B-C and Li-C systems at 100 GPa, the effect of temperature on the structural stability of LiB_3C, crystallographic data of stable and metastable phases, phonon spectra, the DOS, and the Eliashberg spectral function.

[59] M. G. Zhang, Europhys. Lett. **114**, 16001 (2016).

[60] D. E. Bugaris, M. Sturza, F. Han, J. Im, D. Y. Chung, A. J. Freeman, and M. G. Kanatzidis, Eur. J. Inorg. Chem. **2015**, 2164 (2015).

[61] F. Rullier-Albenque, D. Colson, A. Forget, P. Thuéry, and S. Poissonnet, Phys. Rev. B **81**, 224503 (2010).

[62] M. Dogan, S. Oh, and M. L. Cohen, Phys. Rev. B **105**, L020509 (2022).

[63] A. M. Shipley, M. J. Hutcheon, R. J. Needs, and C. J. Pickard, Phys. Rev. B **104**, 054501 (2021).